Journal of Computational Mathematics
Vol.31, No.5, 2013, 449–469.

http://www.global-sci.org/jcm
doi:10.4208/jcm.1304-m3983

FAST ACOUSTIC IMAGING FOR A 3D PENETRABLE OBJECT IMMERSED IN A SHALLOW WATER WAVEGUIDE*

Ju Qiu Zhongbo Zhang
Mathematical School, Jilin University, Changchun 130000, China
Email: qiuju@jlu.edu.cn zhongbozhang@jlu.edu.cn
Wenfeng Pan
School of Science, Wuhan University of Technology, Wuhan 430070, China
Email: panskys@gmail.com

Abstract

The paper is concerned with the inverse problem for reconstructing a 3D penetrable object in a shallow water waveguide from the far-field data of the scattered fields with many acoustic point source incidences. An indicator sampling method is analyzed and presented for fast imaging the size, shape and location of such a penetrable object. The method has the advantages that a priori knowledge is avoided for the geometrical and material properties of the penetrable obstacle and the much complicated iterative techniques are avoided during the inversion. Numerical examples are given of successful shape reconstructions for several 3D penetrable obstacles having a variety of shapes. In particular, numerical results show that the proposed method is able to produce a good reconstruction of the size, shape and location of the penetrable target even for the case where the incident and observation points are restricted to some limited apertures.

Mathematics subject classification: 35R25, 35P25, 76Q05, 65M30, 81U40.
Key words: Oceanic waveguide, Penetrable object, Inverse problems, Indicator sampling method.

1. Introduction

The inverse domain problem of determining the shape of an unknown object from the knowledge of some scattered far-field patterns has drawn considerable attention in recent years due to its importance in many areas of science and technology. It is well-known that this inverse problem is not only nonlinear, but also severely improperly posed in the sense of Hadamard [1]. This means that the numerical solution of such an inverse problem is considerably difficult due to the fact that small perturbations of the far-field pattern can induce large errors in the determination of the shape of the obstacle. During the last two decades, various computational schemes have been developed for solving the inverse domain problem, such as nonlinear optimization or Newton-type iteration techniques [2], linear or indicator sampling methods [3-7], but such efforts focused primarily on the numerical solution for the inverse domain problem in a free space. More to the point, recent works on imaging penetrable objects in free-space, half-space and waveguides, some potential methods such as MUSIC-type algorithms and topological derivative based imaging inhomogeneities of small diameter look like very valuable [8-11], At the same time, analysis of resolution and stability with respect to measurement as well as medium

* Received December 18, 2011 / Revised version received April 1, 2013 / Accepted April 16, 2013 / Published online August 27, 2013 /

noise of the imaging algorithms were performed there. On the other hand, Multistatic imaging of extended targets has been studied in [12].

As well known, the seas occupying more than two-thirds of the surface of the earth are places where a great variety of natural and man-made objects (such as sea mounts, mineral deposits, submarines, sunken vessels, leaky pipelines, submerged wreckage and navigational obstacles, etc.) are located. Acoustic waves are considered as the best tool to identify these objects due to its good propagation in water. Therefore, the inverse domain problem of identifying size, shape and location of an unknown object immersed in a water-filled guide from the scattered far-field information of known acoustic waves has received fairly considerable attention due to its considerable archeological, history and geophysical interest.

Some earlier schemes for solving the inverse domain problem by an impenetrable object in a shallow water waveguide are rather computer-intensive due to the fact that all of them are based on both some nonlinearized iterative techniques and some approximations to the solution of associated direct problem during the inversion[13-15]. Another scheme in this area is the so-called ICD method which is achieved by employing the intersecting canonical domain(ICD) approximation procedure to invert the field in a numerically more efficient manner[16-18]. However, the ICD method has a main disadvantage of being only applicable for the case of a cylindrically axisymmetric object.

It should be emphasized that in these schemes mentioned above, the prior knowledge of what kind of boundary condition on the unknown object is required. However, in practice, the prior information is not available. In order to avoid such an inherent defect in the previously mentioned schemes, a generated dual space indicator method[19-21] was introduced for imaging an impenetrable obstacle having any shape in a shallow water waveguide, which is achieved by the observation that the combination of the measured scattered field can approximate the waveguide Green's function very well when the source point of the waveguide Green's function is inside of the obstacle, but not so well when the source point is outside of the obstacle.

The paper is concerned with the inverse domain problem of the identification of a 3D penetrable object immersed in a shallow water waveguide with perfectly reflecting boundaries. This concern is motivated by the fact that in practice, the scattering object often is a penetrable inclusion, whose material properties differ from those in the surrounding fluid. To our knowledge, no investigation has been reported for the acoustic imaging of a 3D penetrable obstacle placed in a shallow water waveguide.

An indicator sampling method is introduced for solving the inverse penetrable obstacle problem in a shallow water waveguide, which belongs to a further development of a new group of fast acoustic imaging schemes for the inverse domain problem in a free space, good examples of which are found in [5-7]. The main contributions of the indicator sampling method are that its computational speed is rather fast, its implementation is computationally simple and it is no need for a priori information about the scattering object. However, the numerical solution for such an inverse domain problem in a shallow water waveguide does pose particularly challenging difficulties due to the filtering out high-spatial-frequency components of the scattered wavefield with range and the propagation of only finitely many modes[16].

The paper is organized as follows. In Section 2 the basis of the indicator sampling method is analyzed and presented for fast imaging a 3D penetrable object in a shallow water waveguide. In Section 3 the good efficiency of the proposed method is confirmed through a few numerical examples for several 3D penetrable obstacles having a variety of shapes from synthetic far-field data. The last section gives some conclusions and remarks.

2. Indicator Sampling Method

Let $R_h^3 = \{(x,z)\,|x = (x_1,x_2) \in R^2, 0 \le z \le h\}$ be the region occupied by a homogeneous constant depth ocean with a pressure release surface and a rigid bottom, where h is the ocean depth. Assume that the incident wave is normal mode wave with source point(d, z_0), i.e., it may be expressed as [21]

$$u^i(x,z;d,z_0) = \sum_{n=1}^{N} \phi_n(z)\phi_n(z_0)e^{ik_n x\cdot d}. \tag{2.1}$$

Where $N = [(2kh+1)/2\pi]$ is the total number of the propagation modes, and [] denotes the integer part of the term, $\phi_n(z) = \sqrt{2/h}\sin\gamma_n z$, $n = 1,\cdots,$ $\gamma_n = (2n-1)\pi/2h$, $k_n = \sqrt{k^2-\gamma_n^2}$, k is the wavenumber, $z_0$is a fixed number, $0 \le z_0 \le h$, d is a fixed vector, $|d| = 1$.

We should note that the incident wave (2.1) is the propagation far-field pattern of the following Green's function for $|\xi| \to +\infty$

$$G(z,z_0,|x-\xi|) = \frac{i}{4}\sum_{n=1}^{\infty} \phi_n(z)\phi_n(z_0)H_0^{(1)}(k_n|x-\xi|). \tag{2.2}$$

Therefore, the incident wave only consists of finitely propagation (i.e., nonevanescent) modes.

Let D be a bound, simply connected domain in R_h^3 with a boundary ∂D in Hölder class $C^{2,\sigma}$, $0 < \sigma \le 1$, having unit outward normal ν. Denote the exterior domain of D by $D_e = R_h^3 \backslash \bar{D}$. Assume that the acoustic constants of D differ from those of the surrounding medium inD_e. Then there have a scattered field u^s in the exterior domain D_e and a transmission field u_i in D when the incident wave (2.1) impinges on the penetrable object D. Denote the total field in D_e by $u_e = u^i + u^s$, then the direct transmission problem, is to find two functions $u_e \in C^2(D_e) \cap C(\bar{D}_e)$ and $u_i \in C^2(D) \cap C(\bar{D})$ such that

$$\Delta u_e + k^2 u_e = 0 \ \text{ in } D_e, \tag{2.3}$$

$$\Delta u_i + k_i^2 u_i = 0 \ \text{ in } \ D, \tag{2.4}$$

$$u_e = u_i \ \text{ on } \ \partial D, \tag{2.5}$$

$$\frac{\partial u_e}{\partial \nu} = \rho\frac{\partial u_i}{\partial \nu} \ \text{ on } \ \partial D, \tag{2.6}$$

$$u_e|_{z=0} = 0, \frac{\partial u_e}{\partial z}|_{z=h} = 0, \tag{2.7}$$

where k_i the wavenumber in D, ρ is the density ratio.

Note that the scattered wave u^s has the normal modal representation

$$u^s = \sum_{n=1}^{+\infty} \phi_n(z)u_n^s(x) \ \text{ for } \ |x| \gg 1, \tag{2.8}$$

where $(y,\varsigma) \in D_e$ is the nth normal propagation mode of u^s, and it is required to satisfy the outgoing radiation condition

$$\lim_{r\to+\infty} r^{1/2}\Big(\frac{\partial u_n^s}{\partial r} - ik_n u_n^s\Big) = 0, \qquad n = 1,2,\cdots, r = |x|\,. \tag{2.9}$$

To reformulate the inverse problem, we need the uniqueness result of the direct transmission problems (2.3)-(2.7) and (2.9).

Suppose that there were two solutions to the direct transmission problems (2.3)-(2.7) and (2.9), call them $((u_e^1, u_i^1)$ and (u_e^2, u_i^2), and then let $U_e = u_e^1 - u_e^2$ and $U_i = u_i^1 - u_i^2$. Clearly, U_e satisfies (2.3) and (2.7) in D_e and the radiation condition (2.9), U_i satisfies (2.4) in D, and (U_e, U_i) satisfies the interface conditions (2.5 and (2.6). We denote a column centered at origin point with radius R by $\Omega_R := D_e \cap \{(x,z) \in R_h^3, |x| < R\}$ and its surface by S_R. We assume that the radius R is sufficiently large so that D is completely contained in S_R.

Applying the divergence theorem for U_e, U_i and using the transmission conditions we obtain

$$\begin{aligned}\int_{S_R} U_e \frac{\partial \bar{U}_e}{\partial \nu} ds &= \int_{\partial D} U_e \frac{\partial \bar{U}_e}{\partial \nu} ds + \int_{\Omega_R \setminus D} (\nabla U_e \cdot \nabla \bar{U}_e + U_e \Delta \bar{U}_e) dx \\ &= \int_{\partial D} \rho U_i \frac{\partial \bar{U}_i}{\partial \nu} ds + \int_{\Omega_R \setminus D} (\nabla U_e \cdot \nabla \bar{U}_e - k^2 |U_e|^2) dx \\ &= \int_D \rho (\nabla U_i \cdot \nabla \bar{U}_i - k_i^2 |U_i|^2) dx + \int_{\Omega_R \setminus D} (\nabla U_e \cdot \nabla \bar{U}_e - k^2 |U_e|^2) dx.\end{aligned} \tag{2.10}$$

We now consider the following cases:

(1) k and k_i are real number. By taking the imaginary part of (2.10), we have

$$Im\Big(\int_{S_R} U_e \frac{\partial \bar{U}_e}{\partial \nu} ds\Big) = 0. \tag{2.11}$$

As U_e satisfies the radiation condition, we have

$$\int_{S_R} U_e \frac{\partial \bar{U}_e}{\partial \nu} ds \to -k \lim_{R \to \infty} \int_{S_R} |U_e|^2 ds = 0, \tag{2.12}$$

whence from Rellich's lemma it implies that $U_e = 0$ in D_e. Thus, $U_e = 0$ and $\partial U_e / \partial \nu = 0$ on ∂D.

(2) k and k_i have positive imaginary parts. In this case, it is readily shown that U_e decays exponentially at infinity. Hence, we have (2.10). When this is combined with (2.10), we take the imaginary part of (2.10) and we deduced that

$$Im\Big(\int_{S_R} U_e \frac{\partial \bar{U}_e}{\partial \nu} ds\Big) \le 0. \tag{2.13}$$

Rellich's lemma then implies that $U_e = 0$ in D_e. Thus, $U_e = 0$ and $\partial U_e / \partial \nu = 0$ on ∂D.

Now the unique continuation principle implies that $U_i = 0$ in D. So we have proved the following uniqueness result.

Theorem 2.1. *Assume that either k and k_i are real number and have positive imaginary parts. Then the direct transmission problems* (2.3)-(2.7) *and* (2.9) *have at almost one solution.*

Applying Green's theorem for the exterior domainD_e, we have

$$u^s(x,z;d,z_0) = \int_{\partial D} \Big(u_e(\xi,\varsigma;d,z_0) \frac{\partial G(z,\varsigma,|x-\xi|)}{\partial \upsilon(\xi,\varsigma)} - G(z,\varsigma,|x-\xi|) \frac{\partial u_e(\xi,\varsigma;d,z_0)}{\partial \upsilon(\xi,\varsigma)} \Big) ds(\xi,\varsigma). \tag{2.14}$$

It can be obtained from the asymptotic behaviour of Hankel's function and (2.14) that

$$u^s(x,z;d,z_0) = \frac{e^{i\pi/4}}{4} \sum_{n=1}^{N} \sqrt{\frac{2}{\pi k_n r}} e^{ik_n r} u_n^\infty(\hat{x},z;d,z_0) + O\left(\frac{1}{r^{3/2}}\right) \tag{2.15}$$

where

$$\begin{aligned} &u_n^\infty(\hat{x}, z; d, z_0) \\ &= \phi_n(z) \int_{\partial D} \Big(u_e(\xi, \varsigma; d, z_0) \frac{\partial (e^{-ik_n \hat{x}\cdot\xi} \phi_n(\varsigma))}{\partial \upsilon(\xi, \varsigma)} - (e^{-ik_n \hat{x}\cdot\xi} \phi_n(\zeta)) \frac{\partial u_e(\xi, \varsigma; d, z_0)}{\partial \upsilon(\xi, \varsigma)} \Big) ds(\xi, \varsigma). \quad (2.16) \end{aligned}$$

Let the function $u^\infty(\hat{x}, z; d, z_0)$ be defined as

$$u^\infty(\hat{x}, z; d, z_0) = \sum_{n=1}^{N} u_n^\infty(\hat{x}, z; d, z_0), \tag{2.17}$$

where $u^\infty(\hat{x}, z; d, z_0)$ is called the propagation far-field pattern of the scattered field u^s, and $u_n^\infty(\hat{x}, z; d, z_0)$ the far-field pattern of the nth normal propagation mode of the scattered field u^s, which are both defined on the unit cylinder surface Γ with height h, where $\Gamma = \partial B \times [0, h]$ with the unit circle ∂B.

Let us denote the set of the observation points of the propagation far-field pattern by $\Omega = \{(\hat{x}_l, z_m) \in \Gamma \,|\, l = 1, \cdots, L_1, m = 1, \cdots, M_1\}$ and the set of the source points of the incident field by $\Lambda = \{(d_l, z_{0,m}) \in \Gamma \,|\, l = 1, \cdots, L_2, m = 1, \cdots, M_2\}$. Then the inverse problem we are interested in is, given the exterior wavenumber k, to imaging the support of the penetrable object D from the knowledge of the propagation far-field data $u^\infty(\hat{x}, z; d, z_0)$ for $(d, z_0) \in \Omega$ and $(d, z_0) \in \Lambda$.

We now begin with the analysis for solving the inverse transmission problem described above. To this end, let us introduce the following function

$$V(\hat{x}, z; \xi, \eta) = \sum_{n=1}^{N} \phi_n(z) \phi_n(\eta) e^{-ik\hat{x}\cdot\xi}. \tag{2.18}$$

Then we can conclude from (2.16) - (2.17) that

$$u^\infty(\hat{x}, z; d, z_0) = \int_{\partial D} \Big(u_e(\xi, \eta) \frac{\partial V(\hat{x}, z; \xi, \eta)}{\partial \nu} - V(\hat{x}, z; \xi, \eta) \frac{\partial u_e(\xi, \eta)}{\partial \nu} \Big) ds(\xi, \eta), \tag{2.19}$$

where we have omitted the dependence of the total field u_e on the incident source point (z, d_0).

Now, from (2.19) we can obtain

$$\sum_{l=1}^{L_1} \sum_{m=1}^{M_1} g_{lm} u^\infty(\hat{x}_l, z_m; d, z_0) = \int_{\partial D} \Big(u_e(\xi, \eta) \frac{\partial v_g(\xi, \eta)}{\partial \nu} - v_g(\xi, \eta) \frac{\partial u_e(\xi, \eta)}{\partial \nu} \Big) ds(\xi, \eta), \tag{2.20}$$

where g_{lm}, $l = 1, \cdots, L_1, m = 1, \cdots, M_1$ are complex constants, and

$$v_g(\xi, \eta) = \sum_{l=1}^{L_1} \sum_{m=1}^{M_1} g_{lm} V(\hat{x}_l, z_m; \xi, \eta), \tag{2.21}$$

and note that v_g is an entire solution of the Helmholtz equation in R_h^3. Functions of the form (2.21) are called the discrete waveguide Herglotz wavefunctions and the complex vector $g = (g_{lm} | l = 1, \cdots, L_1; m = 1, \cdots, M_1)^T$ is called the discrete Herglotz kernel [22-23].

Let (y, ς) be a given point in D and assume that there exists a complex vector g such that v_g satisfies the interior transmission problem

$$\Delta v + k^2 v = 0 \ \text{ in } D, \tag{2.22}$$

$$\Delta w + k_i^2 w = 0 \quad \text{in } D, \tag{2.23}$$

$$w(x,z) - v(x,z) = G(x,z;y,\varsigma) \quad (x,z) \in \partial D, \tag{2.24}$$

$$\rho \frac{\partial w}{\partial \nu}(x,z) - \frac{\partial v}{\partial \nu}(x,z) = \frac{\partial G}{\partial \nu}(x,z;y,\varsigma) \quad (x,z) \in \partial D. \tag{2.25}$$

Note that when k is not an interior transmission eigenvalue for D, the above interior transmission problem is uniquely solvable and the solution continuously depends on the boundary data.

Now assume that the interior transmission problem (2.22)-(2.25) has a solution (v_g, w) such that v_g is a discrete waveguide Herglotz wavegunction with the discrete Herglotz kernel g. Then, it follows from (2.5), (2.6), (2.20), (2.24) and (2.25) that

$$\begin{aligned}
\sum_{l=1}^{L_1}\sum_{m=1}^{M_1} g_{lm} u^\infty(\hat{x}_l, z_m; d, z_0) &= \int_{\partial D} (u_i \frac{\partial v_g}{\partial \nu} - \rho v_g \frac{\partial u_i}{\partial \nu}) ds \\
&= \int_{\partial D} [(\rho G \frac{\partial u_i}{\partial \nu} - u_i \frac{\partial G}{\partial \nu}) + \rho(u_i \frac{\partial w}{\partial \nu} - w \frac{\partial u_i}{\partial \nu})] ds \\
&= \int_{\partial D} (G \frac{\partial u_e}{\partial \nu} - u_e \frac{\partial G}{\partial \nu}) ds \\
&= \int_{\partial D} [(G \frac{\partial u^i}{\partial \nu} - u^i \frac{\partial G}{\partial \nu}) + (G \frac{\partial u^s}{\partial \nu} - u^s \frac{\partial G}{\partial \nu})] ds \\
&= \int_{\partial D} [G \frac{\partial u^i}{\partial \nu} - u^i \frac{\partial G}{\partial \nu}] ds \\
&= u^i(y, \varsigma; d, z_0),
\end{aligned} \tag{2.26}$$

where we use the following relations

$$\int_{\partial D} \Big(u_i \frac{\partial w}{\partial \nu} - w \frac{\partial u_i}{\partial \nu}\Big) ds = 0, \quad \int_{\partial D} \Big(u^s \frac{\partial G}{\partial \nu} - G \frac{\partial}{\partial \nu} u^s\Big) ds = 0, \tag{2.27}$$

which can be derived from the Green' theorem.

Applying the far-field reciprocity relation, we have from (2.25) that

$$\sum_{l=1}^{L_1}\sum_{m=1}^{M_1} g_{lm} u^\infty(\hat{x}, z; -\hat{x}_l, z_m) = u^i(y, \varsigma; -\hat{x}, z), \quad (\hat{x}, z) \in \Gamma. \tag{2.28}$$

Eq. (2.28) is a one-parameter family of equations about the point $(y, \varsigma) \in R_h^3$. The basis of our indicator sampling method for solving the inverse transmission problem described previously is the analysis of the behavior of the solutions g for all possible positions of the point (y, ς). We note that the previous analysis has shown that if there exists a solution (v, w) of the interior transmission problem (2.22)-(2.25) such that v coincides with a discrete waveguide Herglotz wavefunction v_g having g as its discrete Heglotz kernel, then (2.28) has an exact solution. The following theorem shows that if an exact solution to (2.28) does exist then it is unique.

Theorem 2.2. *Let $\{(\hat{x}_l, z_m)\}_{l=1,m=1}^{l=L_1,m=M_1}$ be any finite set of distinct points in Γ. If k is not an interior transmission eigenvalue for D, then the functions $u^\infty(\hat{x}, z; -\hat{x}_l, z_m)$are linearly independent in $L^2(\Gamma)$ for $l = 1, \cdots, L_1$, $m = 1, \cdots, M_1$.*

Proof. It is sufficient to show that if

$$U^\infty(\hat{x}, z) = \sum_{l=1}^{L_1}\sum_{m=1}^{M1} c_{lm} u^\infty(\hat{x}, z; -\hat{x}_l, z_m) = 0, \quad (\hat{x}, z) \in \Gamma, \tag{2.29}$$

for some choice of constants c_{lm}, $l = 1, \cdots, L_1$, $m = 1, \cdots, M_1$, then $c_{lm} = 0$, $l = 1, \cdots, L_1$, $m = 1, \cdots, M_1$. To this end, we introduce the following functions

$$U^i(x,z) = \sum_{l=1}^{L_1} \sum_{m=1}^{M1} c_{lm} u^i(x,z;-\hat{x}_l, z_m), \tag{2.30}$$

$$U^s(x,z) = \sum_{l=1}^{L_1} \sum_{m=1}^{M1} c_{lm} u^s(x,z;-\hat{x}_l, z_m), \tag{2.31}$$

$$U_i(x,z) = \sum_{l=1}^{L_1} \sum_{m=1}^{M1} c_{lm} u_i(x,z;-\hat{x}_l, z_m). \tag{2.32}$$

It is clear to see that the equations (2.30)-(2.32) are superpositions of the incident, scattered and transmission fields respectively. We note that U^s is a radiation solution of the Helmholtz equation in D_e, and U^∞ is its propagation far-field pattern. Now, the Rellich' lemma [24] yields that $U^s = 0$ in D_e, and hence $U^s = 0$ on ∂D. Therefore, from (2.5) and (2.6), we can conclude that the pair (U^i, U_i) solves the homogeneous interior transmission problem. The fact that k is not an interior transmission eigenvalue for D now follows that $U^i = 0$ in D. We note that U^i is an entire solution of the Helmholtz equation in R^3_h and is analytic in R^3_h, and hence the unique continuation yields that

$$\sum_{l=1}^{L_1} \sum_{m=1}^{M_1} c_{lm} u^i(x,z;-\hat{x}_l, z_m) = 0 \ \text{ in } \ R^3_h. \tag{2.33}$$

Then we have from (2.33) that

$$\sum_{l=1}^{L_1} \sum_{m=1}^{M_1} c_{lm} u^i(\xi_l, z_m;-\hat{x}, z) = 0 \ \text{ on } \ \Gamma, \tag{2.34}$$

where $\xi_l = R_0 \hat{x}_l$, R_0 is a positive constant. We introduce a function U by

$$U(x,z) = \sum_{l=1}^{L_1} \sum_{m=1}^{M_1} c_{lm} G(x,z;\xi_l, z_m), \ (x,z) \in R^3_n \backslash \{\xi_l, z_m\}_{l=1,m=1}^{l=L_1,m=M_1}. \tag{2.35}$$

Note that $U(x,z)$ is a radiation solution of the Helmholtz equation in R^3_h and is analytic in $R^3_h \backslash \{\xi_l, \eta_m\}_{l=1,m=1}^{l=L_l,m=M_1}$. Now the asymptotic behavior of the Hankel function yields that the left side of (2.34) is the propagation far-field pattern of the radiation solution U, and hence $U = 0$ in R^3_h. As in the proof of Lemma 4.1 of [25], we can now conclude that $c_{lm} = 0$, $l = 1, \cdots, L_1$, $m = 1, \cdots, M_1$. □

We now turn to our main goal, that is to analyze the behavior of the solutions to the equation (2.28) for various sampling points $(y, \varsigma) \in R^3_h$. Let us emphasize that a particular challenging for achieving this goal is that an exact solution to (2.28) may not exist due to the fact that there may not exist a solution (v, w) of the interior transmission problem (2.22)-(2.25) such that v is a discrete waveguide Herglotz wavefunction. Therefore, we can only try to find a complex vector g such that (2.28) is approximately satisfied within an arbitrary prescribed error in the maximum norm. To this end, we have to introduce the following spaces:

$$X = span \left\{ \sum_{n=1}^{N} \phi_n(z) \phi_n(\eta_m) e^{ik_n x \cdot \hat{\xi}_l} : (\hat{\xi}_l, \eta_m) \in \Gamma, l, m = 1, 2, \cdots \right\}, \tag{2.36}$$

$$Y = \left\{ w \in H^1(\bar{D}), \Delta w + k_i^2 w = 0, \text{in } D \right\}, \tag{2.37}$$

$$W = \left\{ \left((h-w)|_{\partial D}, \frac{\partial}{\partial \nu}(h - \rho w) \right) : h \in X, w \in Y \right\}. \tag{2.38}$$

We then have the following theorem.

Theorem 2.3. *Let $\{(\hat{\xi}_l, \eta_m)\}_{l=1,m=1}^{l=\infty,m=\infty}$ be a sequence of distinct points that is dense in Γ. If k is not an interior transmission eigenvalue for D, Then W is complete in $H(\partial D)$, where $H(\partial D) = H^{1/2}(\partial D) \times H^{-1/2}(\partial D)$.*

Proof. Suppose that for any $h \in X$ and $w \in Y$, there exist $\varphi \in H^{1/2}(\partial D)$ and $\psi \in H^{-1/2}(\partial D)$ such that

$$\int_{\partial D} \left[(h-w)\bar{\varphi} + \frac{\partial}{\partial \upsilon}(h - \rho w)\bar{\psi} \right] ds = 0. \tag{2.39}$$

Then it suffices to show that $\varphi = \psi = 0$. To this end, we define v^∞ by

$$v^\infty(\hat{\xi}, \eta) = \sum_{n=1}^{N} \phi_n(\eta) \int_{\partial D} \left[\bar{\varphi}\phi_n(z) e^{-ik_n x\cdot\hat{\xi}} + \bar{\psi}\frac{\partial}{\partial \nu}\phi_n(z) e^{-ik_n x\cdot\hat{\xi}} \right] ds(x,z), \tag{2.40}$$

and note that v^∞ is an analytic function on Γ. We now have from (2.39) with $w = 0$ that

$$v^\infty(\hat{\xi}_l, \eta_m) = 0, l, \quad m = 1, 2, \cdots. \tag{2.41}$$

By the unique continuation, the fact that the sequence $\{(\hat{\xi}_l, \eta_m)\}_{l=1,m=1}^{l=\infty,m=\infty}$ is dense in Γ yields that $v^\infty(\hat{\xi}, \eta) = 0$ for all $(\hat{\xi}, \eta) \in \Gamma$. Define a function v by

$$v(\xi, \eta) = \int_{\partial D} \left[\bar{\varphi} G(\xi, \eta; x, z) + \bar{\psi}\frac{\partial}{\partial \nu} G(\xi, \eta; x, z) \right] ds(x,z), \quad (\xi, \eta) \in R_h^3 \backslash \partial D. \tag{2.42}$$

Then v is a radiation solution of the Helmholtz equation in $R_h^3 \backslash \bar{D}$ having the propagation far-field pattern $v^\infty(\hat{\xi}, \eta) = 0$ for all $(\hat{\xi}, \eta) \in \Gamma$. By Rellich's Lemma, we can conclude that $v = 0$ in $R_h^3 \backslash \bar{D}$, and hence $v = 0$ on ∂D. It follows from the continuity properties of the double and single layer potentials that

$$v_- = -\bar{\psi}, \quad \frac{\partial v_-}{\partial \nu} = \bar{\varphi} \ \text{ on } \partial D, \tag{2.43}$$

where the minus subscript denotes the limit as x tends to ∂D from D. We define γ_n^j by

$$\gamma_n^j = \phi_n(z) J_j(k_{i,n} r_x) e^{-ij\theta_x}, \quad j = 0, \pm 1, \cdots, \ n = 1, \cdots, \tag{2.44}$$

where $k_{i,n} = \sqrt{k_i^2 - \lambda_n^2}$, and (r_x, θ_x) is the polar coordinate of x. We note that $\gamma_n^j \in Y$, and hence we have from (2.39) with $h = 0$ that

$$\int_{\partial D} \left[\gamma_n^j \bar{\varphi} + \rho \frac{\partial \gamma_n^j}{\partial \nu} \bar{\psi} \right] ds = 0, \quad j = 0, 1, \cdots, \quad n = 1, \cdots. \tag{2.45}$$

From the additional formula for Hankel functions

$$H_0^{(1)}(k_{i,n}|x - \xi|) = \sum_{j=-\infty}^{+\infty} H_j^{(1)}(k_{i,n} r_\xi) J_j(k_{i,n} r_x) e^{ij(\theta_\xi - \theta_x)}, \quad r_\xi > r_x, \tag{2.46}$$

where (r_ξ, θ_ξ) is the polar coordinate of ξ, we have that the function u defined by

$$u(\xi,\eta) = \int_{\partial D} \left[\bar{\varphi} G_i(\xi,\eta;x,z) + \rho\bar{\psi}\frac{\partial}{\partial\nu} G_i(\xi,\eta;x,z)\right] ds(x,z), \quad (\xi,\eta) \in R_h^3 \backslash \partial D, \tag{2.47}$$

is identically zero in $R_h^3 \backslash \bar{D}$, where

$$G_i(\xi,\eta;x,z) = \frac{i}{4}\sum_{n=1}^{\infty} \phi_n(z)\phi_n(\eta) H_n^{(1)}(k_{i,n}|x-\xi|). \tag{2.48}$$

We have from the continuity properties of the double and single layer potentials that

$$u_- = -\rho\bar{\psi}, \quad \frac{\partial u_-}{\partial\nu} = \bar{\varphi} \ \text{ on } \ \partial D, \tag{2.49}$$

and then it follows from (2.39) and (2.45) that

$$\rho v_- - u_- = 0, \quad \frac{\partial v_-}{\partial\nu} - \frac{\partial u_-}{\partial\nu} = 0 \ \text{ on } \ \partial D. \tag{2.50}$$

Therefore, the pair $(\rho v|_D, u_0|_D)$ is the solution of the homogenous interior transmission problem. Since k is not an interior transmission eigenvalue for D, we conclude that $v = 0$ in D. It follows from (2.43) that $\varphi = 0, \psi = 0$, and hence W is complete in $H(\partial D)$. □

Theorem 2.3 means that when $(y,\varsigma) \in D$, for every $\varepsilon > 0$ there exists a discrete waveguide Herglotz wavefunction $v_{g^\varepsilon}(\cdot;y,\varsigma) \in X$ with a discrete Herglotz kernel g^ε and a function $w \in Y$ such that

$$\begin{aligned}&\left\|w(\cdot;y,\varsigma) - v_{g^\varepsilon}(\cdot;y,\varsigma) - G(\cdot;y,\varsigma)\right\|_{L^2(\partial D)} \\ &\quad + \left\|\frac{\partial}{\partial\nu}\Big(\rho w(\cdot;y,\varsigma) - v_{g^\varepsilon}(\cdot;y,\varsigma) - G(\cdot;y,\varsigma)\Big)\right\|_{L^2(\partial D)} < \varepsilon.\end{aligned} \tag{2.51}$$

Now, we introduce the following functions

$$U_g^s = \sum_{l=1}^{L_1}\sum_{m=1}^{M_1} g_{lm}^\varepsilon(y,\varsigma) u^s(x,z;-\hat{x}_l,z_m), \tag{2.52}$$

$$U_{g,i} = \sum_{l=1}^{L_1}\sum_{m=1}^{M_1'} g_{lm}^\varepsilon(y,\varsigma) u_i(x,z;-\hat{x}_l,z_m). \tag{2.53}$$

Note that $(U_g^s, U_{g,i})$ is the solution of the direct transmission problem (2.3)-(2.7) satisfying the outgoing radiation condition (2.9) having the discrete waveguide Heglotz wavefunction $v_{g^\varepsilon}(\cdot;y,\varsigma)$ with the discrete Herglotz kernel g^ε as the incident field, and the left-hand side of (2.28) is the propagation far-field pattern of the radiation solution U_g^s. Therefore, it follows from (2.5) and (2.6) that

$$\begin{aligned}&\left\|[U_g^s - G(\cdot;y,\varsigma)] - [U_{g,i} - w(\cdot;y,\varsigma)]\right\|_{L^2(\partial D)} \\ &\quad + \left\|\frac{\partial}{\partial\nu}\Big(U_g^s - G(\cdot;y,\varsigma)] - \rho[U_{g,i} - w(\cdot;y,\varsigma)\Big)\right\|_{L^2(\partial D)} < \varepsilon.\end{aligned} \tag{2.54}$$

We note that the radiation Green's function $G(x,z;y,\varsigma)$ has the propagation far-field pattern $u^i(y,\varsigma;-\hat{x},z)$, and hence the fact that the propagation far-field pattern of the radiation solution

of the direct transmission problem continuously depends on the boundary data yields that there exists a positive constant C, independent of ε, such that

$$\lim_{(\hat{x},z)\in\Gamma}\left|\sum_{l=1}^{L_1}\sum_{m=1}^{M_1} g_{lm}^{\varepsilon}(y,\varsigma)u^{\infty}(\hat{x},z;-\hat{x}_l,z_m)-u^i(y,\varsigma;-\hat{x},z)\right|\leq C\varepsilon. \tag{2.55}$$

In the following, we consider the behaviour of g^{ε} when (y,ς)approaches the boundary ∂D from interior of D. To this end, we choose a sequence of points defined by

$$x_p = x^* - \frac{R_1}{p}\nu(x^*)\in D, \qquad p=1,2,\cdots, \tag{2.56}$$

where $x^*\in\partial D$ and $R_1>0$ is a sufficiently small number.

Let (v_p,w_p) be the solution of the interior transmission problem (2.22)-(2.25) corresponding to the given point x_p. Then, by the same arguments as in the case of anisotropic media in free space [21], we can conclude that

$$\lim_{p\to+\infty}||v_p||_{H^1(D)}=+\infty. \tag{2.57}$$

From (2.24), (2.25) and (2.51) it follows that

$$\begin{aligned}&\Big\|(w-w_p)-(v_{g^{\varepsilon}}(\cdot;x_p)-v_p)\Big\|_{L^2(\partial D)}\\&\quad+\Big\|\frac{\partial}{\partial\nu}\Big(\rho(w-w_p)-(v_{g^{\varepsilon}}(\cdot;x_p)-v_p)\Big)\Big\|_{L^2(\partial D)}<\varepsilon,\end{aligned} \tag{2.58}$$

which leads to the fact that the discrete waveguide Herglotz wavefunction $v_{g^{\varepsilon}}(\cdot;x_p)$ can approximate the solution v_p of the interior transmission problem (2.22)-(2.25) corresponding to the given point x_p. Therefore, from (2.57) we obtain

$$\lim_{p\to+\infty}||v_{g^{\varepsilon}}(\cdot;x_p)||_{L^2(\partial D)}=+\infty, \tag{2.59}$$

and hence, from (2.21) it follows that

$$\lim_{p\to+\infty}|g^{\varepsilon}(x_p)|=+\infty, \tag{2.60}$$

where

$$|g^{\varepsilon}(x_p)|=\sqrt{\sum_{l=1}^{L_1}\sum_{m=1}^{M_1}|g_{lm}(x_p)|^2}. \tag{2.61}$$

So far, we have analyzed the behavior of the approximation solutions to the equation (2.28) for sampling points $(y,\varsigma)\in\bar{D}$. Now we turn our attention to the case where $(y,\varsigma)\in R_h^3\backslash\bar{D}$. To this end, we introduce the following general transmission problem, i.e. to find two functions $u\in C^2(D_e)\cap C(\bar{D}_e)$ and $w\in C^2(D)\cap C(\bar{D})$ such that

$$\Delta u+k^2u=0, \qquad \text{in } D_e, \tag{2.62}$$

$$\Delta w+k_i^2w=0, \qquad \text{in } D, \tag{2.63}$$

$$w-u=f, \qquad \text{on } \partial D, \tag{2.64}$$

$$\rho\frac{\partial w}{\partial\nu}-\frac{\partial u}{\partial\nu}=h, \qquad \text{on } \partial D, \tag{2.65}$$

$$u|_{z=0}=0, \qquad \frac{\partial u}{\partial z}|_{z=h}=0, \tag{2.66}$$

where $(f,h) \in H^1(\partial D)$, and the scattered field u is required to satisfy the outgoing radiation condition (2.9).

The boundary operator $B : H_0(\partial D) \to L^2(\Gamma)$is now defined to be the linear operator mapping the boundary data (f,h) onto the propagation far-field pattern u^∞ of the radiation solution u where

$$H_0(\partial D) = \Big\{(v|_{\partial D}, \frac{\partial v}{\partial \nu}|_{\partial D}) : v \in \bar{H}\Big\}, \tag{2.67}$$

$$\bar{H} = \Big\{v \in H^1(D) : \Delta v + k^2 v = 0 \text{ in } D\Big\}. \tag{2.68}$$

Assume that k is not an interior transmission eigenvalue, proceeding as in Theorem 4.3 of [26], we have that the operator B is injective and has dense range in $L^2(\Gamma)$. Now, the fact that the left-hand side of (2.28) is the propagation far-field pattern of the transmission problem (2.3)-(2.7) having the discrete waveguide Herglotz wavefunction v_g as the incident field implies that Eq. (2.24) can be rewritten as

$$B(Hg)(\hat{x},z) = u^i(y,\varsigma;-\hat{x},z), \quad (\hat{x},z) \in \Gamma, \tag{2.69}$$

where

$$Hg = \Big(v_g, \frac{\partial v_g}{\partial \nu}\Big). \tag{2.70}$$

In spite of the fact that the right hand side of (2.68) dose not belong range of the operator B when $(y,\varsigma) \in R_h^3 \backslash \bar{D}$, the fact that the operator B has dense range in $L^2(\Gamma)$ allows us to reconstruct a regularized solution $(f^\alpha, h^\alpha) = (v^\alpha(\cdot;y,\varsigma)|_{\partial D}, \frac{\partial v^\alpha}{\partial \nu}(\cdot;y,\varsigma)|_{\partial D})$ of the following equation

$$B(f,h)(\hat{x},z) = u^i(y,\varsigma;-\hat{x},z), \quad (\hat{x},z) \in \Gamma, \tag{2.71}$$

with the regularized parameter $\alpha > 0$,such that for an arbitrary small but fixed $\delta > 0$, we have

$$||B(f^\alpha,h^\alpha)(\hat{x},z) - u^i(y,\varsigma;\hat{x},z)||_{L^2(\Gamma)} \le \delta, \tag{2.72}$$

$$\lim_{\alpha\to 0}\{||f^\alpha||_{H^{1/2}(\partial D)} + ||h^\alpha||_{H^{-1/2}(\partial D)}\} = \infty. \tag{2.73}$$

By the previous analysis, we have implied that f^α can be approximated in the trace space by the discrete waveguide Herglotz wavefunction $v_g^{\alpha,\varepsilon}(\cdot;y,\varsigma)$ with a discrete Herglotz kernel $g^{\alpha,\varepsilon}(y,\varsigma)$ and from the continuity of B we have

$$||B(Hg^{\alpha,\varepsilon}) - B(f^\alpha,h^\alpha)||_{L^2(\Gamma)} < \varepsilon, \tag{2.74}$$

with ε arbitrary small. From (2.72) and (2.74), we have that

$$\lim_{(\hat{x},z)\in\Gamma}\left|\sum_{l=1}^{L_1}\sum_{m=1}^{M_1} g_{lm}^{\alpha,\delta} u^\infty(-\hat{x},z;-\hat{x}_l,z_m) - u^i(y,\varsigma;-\hat{x},z)\right| < \varepsilon + \delta, \tag{2.75}$$

and from (2.73) and the fact that f^α can be approximated by $v_g^{\alpha,\varepsilon}(\cdot;y,\varsigma)$ in the trace space , it follows that

$$\lim_{\alpha\to 0}||Hg^{\alpha,\varepsilon}||_{H_0(\partial D)} = \infty, \quad \lim_{\alpha\to 0}||v_g^{\alpha,\varepsilon}(\cdot;y,\varsigma)||_{H^1(D)} = \infty. \tag{2.76}$$

Consequently,

$$\lim_{\alpha\to 0}|g^{\alpha,\varepsilon}(y,\varsigma)| = \infty. \tag{2.77}$$

We summarize these results in the following theorem.

Theorem 2.4. *Assume that k is not an interior transmission eigenvalue for D. Let u^∞ be the propagation far-field pattern of the transmission problem* (2.3)-(2.7)*. Then we have that*

1. *If $(y,\varsigma) \in D$ then for every $\varepsilon > 0$ there exists a complex vector $g^\varepsilon(y,\varsigma)$ such that*

$$\lim_{(\hat{x},z)\in\Gamma} \left| \sum_{l=1}^{L_1} \sum_{m=1}^{M_1} g_{lm}^\varepsilon(y,\varsigma) u^\infty(-\hat{x},z;-\hat{x}_l,z_m) - u^i(y,\varsigma;-\hat{x},z) \right| < \varepsilon, \tag{2.78}$$

where $g^\varepsilon(y,\varsigma) = \left\{ g_{lm}^\varepsilon(y,\varsigma) | l = 1,\cdots,L_1, m = 1,\cdots,M_1 \right\}$, and

$$\lim_{(y,\varsigma)\to\partial D} |g^\varepsilon(y,\varsigma)| = \infty. \tag{2.79}$$

2. *If $(y,\varsigma) \in R_h^3 \backslash \bar{D}$ then for every $\varepsilon > 0$ and $\delta > 0$, there exists a complex vector $g^{\varepsilon,\delta}(y,\varsigma)$ such that*

$$\lim_{(\hat{x},z)\in\Gamma} \left| \sum_{l=1}^{L_1} \sum_{m=1}^{M_1} g_{lm}^{\varepsilon,\delta}(y,\varsigma) u^\infty(-\hat{x},z;-\hat{x}_l,z_m) - u^i(y,\varsigma;-\hat{x},z) \right| < \varepsilon + \delta, \tag{2.80}$$

where $g^{\varepsilon,\delta}(y,\varsigma) = \{ g_{lm}^{\varepsilon,\delta}(y,\varsigma) | l = 1,\cdots,L_1, \ \ m = 1,\cdots,M_1 \}$, and

$$\lim_{\delta\to 0} |g^{\varepsilon,\delta}(y,\varsigma)| = \infty. \tag{2.81}$$

The above theorem has a particular importance of being able to motivate an indicator sampling method for solving the inverse domain problem for a 3D penetrable obstacle D from a knowledge of the propagation far-field data $u^\infty(\hat{x},z;d,z_0)$ for $(d,z_0) \in \Omega$ and $(d,z_0) \in \Lambda$. The basic idea of the indicator sampling method is that by using regularization methods to solve the equation (2.28) for various sampling points (y,ς) on an appropriate grid containing D, an approximation to $g(y,\varsigma)$ can be obtained and hence the knowledge of the size, shape and location of the obstacle D can be retrieved by those points where $|g(y,\varsigma)|$is not finite. We suggest that readers refer to [5-7] for detail imaging procedures.

3. Numerical Results

In this section, we will present some results of numerical experiments to rapidly reconstruct the support of a penetrable object immersed in a shallow water waveguide using the proposed indicator sampling method in the previous section.

The data for the inverse problem are the synthetic far-field data $u^\infty(\hat{x},z;d,z_0)$ for $(\hat{x},z) \in \Omega$ and $(d,z_0) \in \Lambda$. These data were generated by approximately solving the direct transmission problem by using a least-squares method. To accomplish this, we approximate the scattered field u^s and the transmitted field u_i by the finite sums of the forms respectively

$$u^s(x,z) = \sum_{s=1}^{S} a_s G(x,z;\xi_s,\eta_s), \quad (x,z) \in D_e, (\xi_s,\eta_s) \in D, \tag{3.1}$$

$$u_i(x,z) = \sum_{l=1}^{L} b_l G_i(x,z;\xi_l,\eta_l), \quad (x,z) \in D, (\xi_l,\eta_l) \in D_e. \tag{3.2}$$

The above two representations contain the unknowns $a_s, s = 1, \cdots, S$ and $b_l, l = 1, \cdots, L$. To determine these unknown coefficients, we need to perform a least-squares fit to the boundary data on ∂D. To this end, we define the minimization problem

$$Q(a,b) = \lim_{a,b} ||u_i - (u^i + u^s)^2_{L^2(\partial D)} + \left\| \frac{\partial}{\partial \upsilon}(\rho u_i - u^i - u^s) \right\|^2_{L^2(\partial D)}, \tag{3.3}$$

where $a = \{a_s\}_{s=1}^S$, $b = \{b_l\}_{l=1}^L$.

Then, the unknown coefficients a_s and b_l in (3.1) and (3.2) can be found by solving the minimization problem (3.3). Having computed an approximation of the complex vector a, by means of the asymptotic form of the Hankel function, we can conclude that the scattered field u^s has the propagation far-field pattern of the form

$$u^\infty(\hat{x}, z, d, z_0) = \sum_{s=1}^{S} a_s \sum_{n=1}^{N} \phi_n(z)\phi_n(\eta_s) e^{-ik_n \hat{x}\cdot\xi_s}.$$

Now, we define the following sets of incident and measured points

$$\begin{aligned}
\Omega_1 &= \left\{(\hat{\mathbf{x}}, z) \middle| \hat{\mathbf{x}} = (\cos\theta, \sin\theta), \theta = \frac{i\pi}{6}, z = \frac{jh}{13}, \quad 0 \le i \le 11, \ \ 1 \le j \le 12\right\},\\
\Omega_2 &= \left\{(\hat{\mathbf{x}}, z) \middle| \hat{\mathbf{x}} = (\cos\theta, \sin\theta), \theta = \frac{i\pi}{11}, z = \frac{jh}{13}, \quad 0 \le i \le 11, \ \ 1 \le j \le 12\right\},\\
\Omega_3 &= \left\{(\hat{\mathbf{x}}, z) \middle| \hat{\mathbf{x}} = (\cos\theta, \sin\theta), \theta = \frac{i\pi}{22}, z = \frac{jh}{13}, \quad 0 \le i \le 11, \ \ 1 \le j \le 12\right\},\\
\Omega_4 &= \left\{(\hat{\mathbf{x}}, z) \middle| \hat{\mathbf{x}} = (\cos\theta, \sin\theta), \theta = \frac{i\pi}{6}, z = \frac{h}{4} + \frac{jh}{22}, \quad 0 \le i \le 11, \ \ 1 \le j \le 11\right\},\\
\Omega_5 &= \left\{(\hat{\mathbf{x}}, z) \middle| \hat{\mathbf{x}} = (\cos\theta, \sin\theta), \theta = \frac{i\pi}{12}, z = \frac{h}{4} + \frac{jh}{22}, \quad 0 \le i \le 11, \ \ 1 \le j \le 11\right\},\\
\Omega_6 &= \left\{(\hat{\mathbf{x}}, z) \middle| \hat{\mathbf{x}} = (\cos\theta, \sin\theta), \theta = \frac{i\pi}{22}, z = \frac{h}{4} + \frac{jh}{22}, \quad 0 \le i \le 11, \ \ 1 \le j \le 11\right\},
\end{aligned}$$

where Ω_1, Ω_2 and Ω_3 denote the full, a half and a quarter of the unit cylinder surface with height h, respectively. Ω_4, Ω_5 and Ω_6 denote the full, a half and a quarter of the unit cylinder surface with height $0.5h$. We also define $\Lambda_m = \Omega_m$.

We consider the following six types of data in numerical tests:

Type I: The incident and received data of the full of the unit cylinder surface with height h: $\Lambda = \Lambda_1$, $\Omega = \Omega_1$;

Type II: The incident and received data of the half of the unit cylinder surface with height h: $\Lambda = \Lambda_2$, $\Omega = \Omega_2$;

Type III: The incident and received data of the quarter of the unit cylinder surface with height h: $\Lambda = \Lambda_3$, $\Omega = \Omega_3$;

Type IV: The incident and received data of the full of the unit cylinder surface with height $0.5h$: $\Lambda = \Lambda_4$, $\Omega = \Omega_4$;

Type V: The incident and received data of the half of the unit cylinder surface with height $0.5h$: $\Lambda = \Lambda_5$, $\Omega = \Omega_5$;

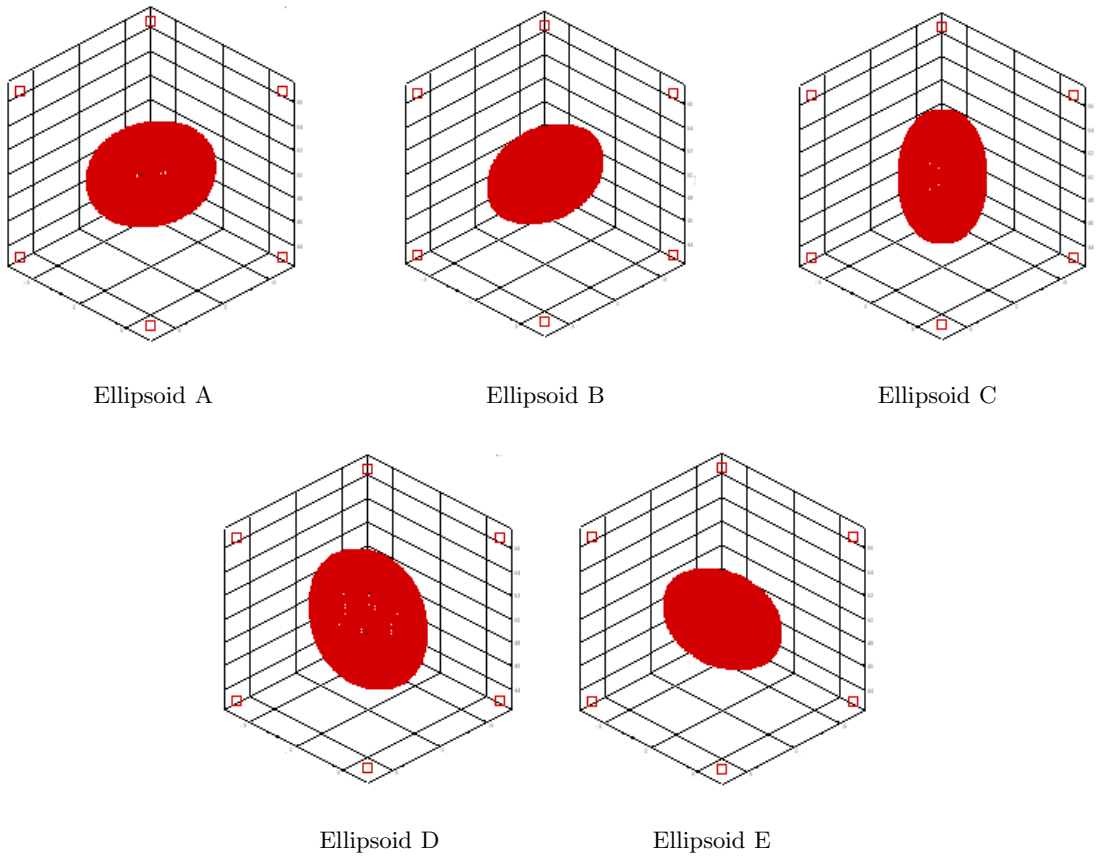

Fig. 3.1. The schematic of the obstacles used in the numerical experiments.

Type VI: The incident and received data of the quarter of the unit cylinder surface with height $0.5h$: $\Lambda = \Lambda_6$, $\Omega = \Omega_6$.

We note that in each case above, the incident acoustic field illuminates the penetrable object from 144 distinct points distributed over the incident domain Λ, and for each point of incidence, the propagation far-field pattern of the scattering field is measured at 144 different observation points distributed over the view domain Ω.

In the numerical computations, the sea depth has taken as $h = 100(m)$, the sampling domain has been taken as a $32 \times 32 \times 32$ grid of the cube $[-7m, 7m]^3$ centered at $(0, 0, h_z)$ in R_h^3. The boundary ∂D of the obstacle we want to reconstruct is given by

$$\partial D = \left\{ (x_1, x_2, z) : \frac{x_1^2}{a^2} + \frac{x_2^2}{b^2} + \frac{(z - h_z)^2}{c^2} = 1 \right\}.$$

Numerical experiments were carried out for the following obstacles, as shown in Fig. 3.1:

(1) Ellipsoid A: $a = 5(m)$, $b = 4(m)$, $c = 3(m)$;

(2) Ellipsoid B: $a = 5(m)$ $b = 3(m), c = 3(m)$;

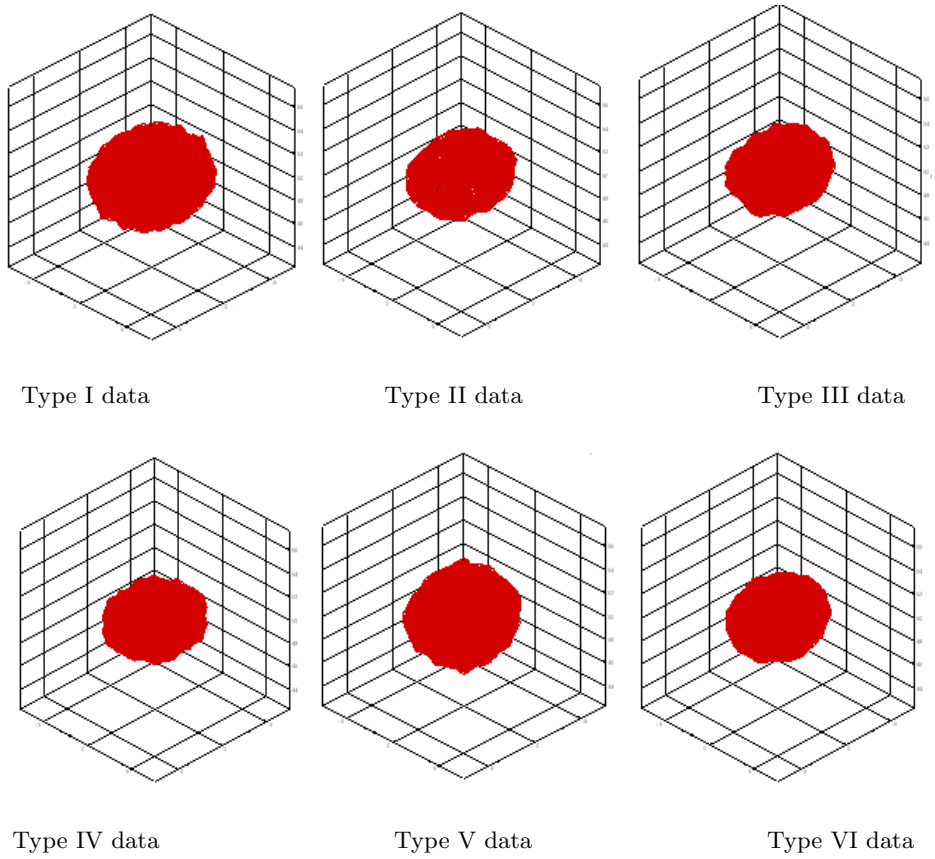

Fig. 3.2. Reconstructions with 2% noise data for the ellipsoid A centered at $(0, 0, h/2)$ based on the type II data, type IV data and type VI data respectively from the left-hand side to the right-hand side. In each case, the exterior wave number $k = 1.5(m^{-1})$, the interior wave number $k_i = 2.0(m^{-1})$ and the density ratio $\rho = 2.0$.

(3) Ellipsoid C: $a = 3(m)$, $b = 2(m)$,$c = 5(m)$;

(4) Ellipsoid D: $a = 3(m)$, $b = 5(m)$, $c = 5(m)$;

(5) Ellipsoid E: $a = 3(m)$, $b = 5(m)$, $c = 3(m)$.

As a first example of numerical applications, we want to exploit the effects of the different incident and measured apertures on the reconstructions, as shown in Fig. 3.2. The reconstructing results are illustrated by the case where the obstacle we want to identify is the ellipsoid A centered at $(0, 0, h/2)$ and the six types of incident and received data are considered. Moreover, for these reconstructions, the wavenumber of the incident wave we use to impinge the unknown object has been taken as $k = 1.5(m^{-1})$, the synthetic far-field data for the inverse problem are obtained by the case where $k_i = 2.0(m^{-1})$ and $\rho = 2.0$. However, let us emphasize that in our inversion procedure, no a priori information is needed for the interior wavenumber k_i and density ratio ρ of the unknown object.

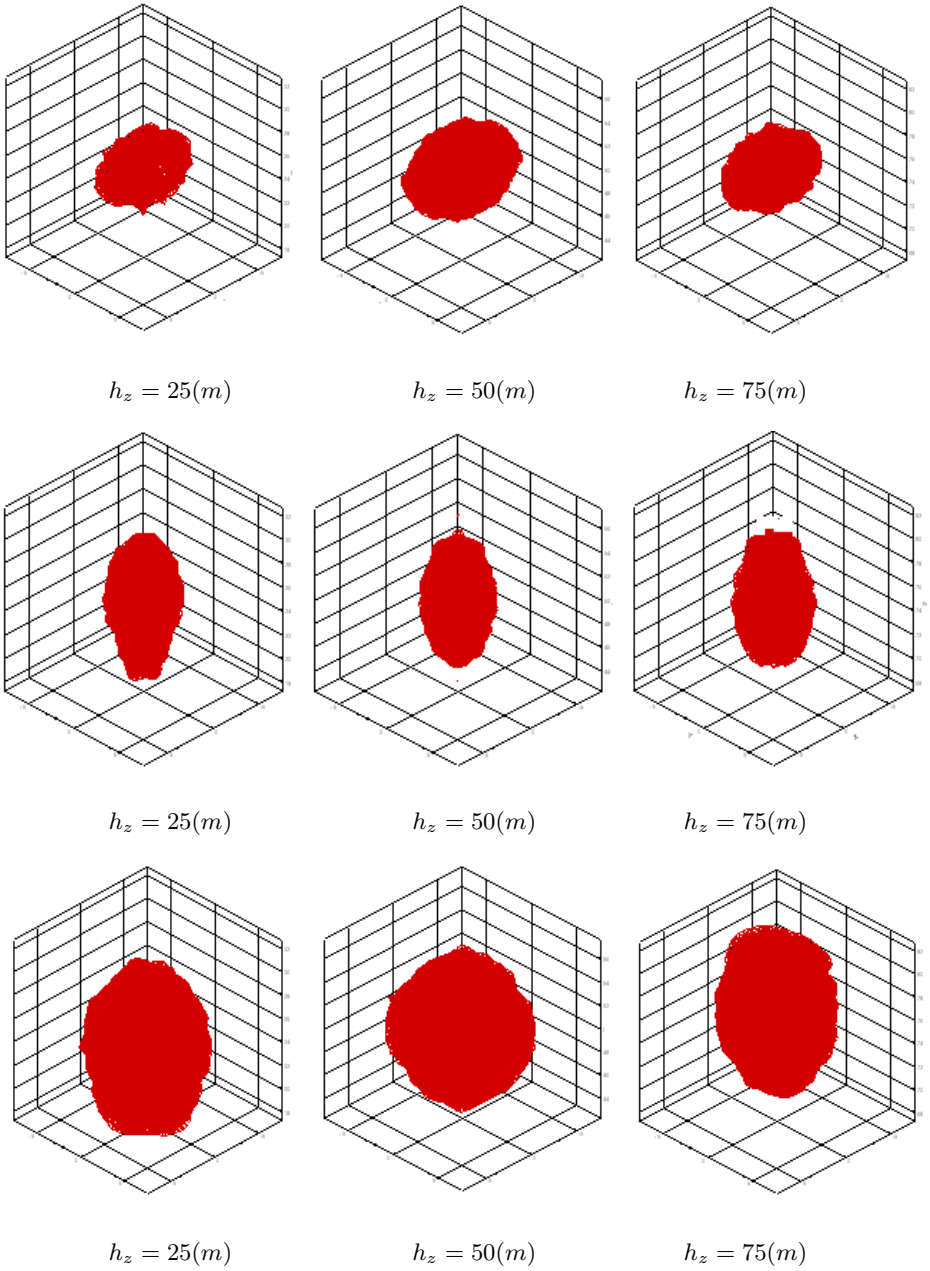

Fig. 3.3. Multiple-scattering effects of the waveguide boundaries on the reconstructions. The top row gives the reconstructions based on the type I data for the ellipsoid B; the middle row gives the reconstructions based on the type III data for the ellipsoid C; the lower row gives the reconstructions based on the type V data for the ellipsoid E. In each case the exterior wave number $k = 1.5(m^{-1})$, the interior wave number $k_i = 2.0(m^{-1})$ and the density ratio $\rho = 2.0$.

The results show that the proposed method has the ability to clearly identify the size, shape and location of the penetrable object immersed in a shallow water in the case of the availability of only aspect-limited far-field data with finitely many modes in the waveguide. However, the

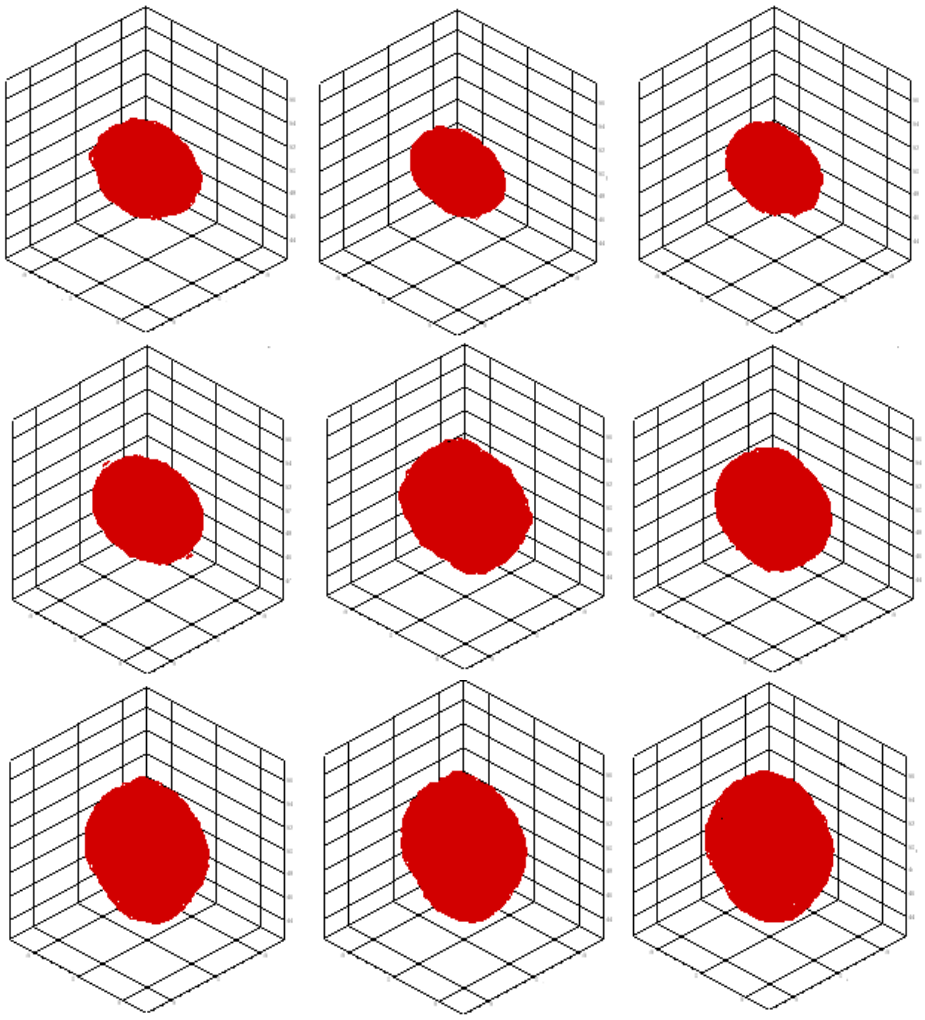

Fig. 3.4. The effects of the exterior wavenumber k, the interior wavenumber k_i and the density ratio ρ on the reconstructions for the ellipsoid D centered at $(0, 0, h/2)$. The top row gives the reconstructions based on the type II data with the interior wavenumber $k_i = 1.5(m^{-1})$, and the density ratio $\rho = 1.5$, the exterior wavenumber $k = 1.0, 2.0, 3.0(m^{-1})$ respectively from the left-hand side to the right-hand side; the middle row gives the reconstructions based on the type IV data with the exterior wavenumber $k = 2.0(m^{-1})$, and the density ratio $\rho = 2.0$, the interior wavenumber $k_i = 1.0, 2.0, 3.0(m^{-1})$ respectively from the left-hand side to the right-hand side; the lower row gives the reconstructions based on the type VI data with exterior wavenumber$k = 3.0(m^{-1})$ and the interior wavenumber $k = 1.5(m^{-1})$, the density ratio $\rho = 2.0, 3.0, 4.0$ respectively from the left-hand side to the right-hand side.

results also indicate that the fidelity of the reconstruction with decreasing the incident and received apertures will be diminished due to the fact that the consequent loss of information leads to the more severely ill-conditioned nature of the far-field matrix in (2.24), and this in turn limits the accuracy of determining the indicator sampling function $g(y, \varsigma)$.

In the following example, we consider the multiple-scattering effects of the waveguide boundaries on the reconstructions. As well known, the complexity of the acoustic propagation in a shallow water is greatly increased due to the presence of both the sea surface and the sea floor.

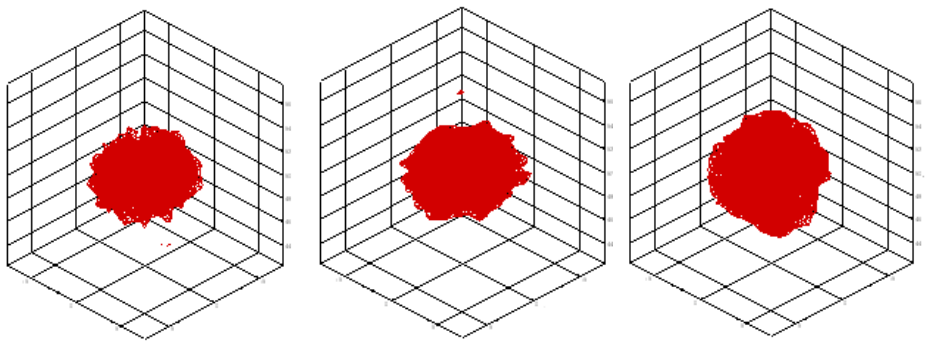

Fig. 3.5. Reconstructions with 2% noise data for the ellipsoid A centered at $(0, 0, h/2)$ based on the type II data, type IV data and type VI data respectively from the left-hand side to the right-hand side. In each case, the exterior wave number $k = 1.5(m^{-1})$, the interior wave number $k_i = 2.0(m^{-1})$ and the density ratio $\rho = 2.0$.

In general, the multiple-scattering effects will be strong when the scattering obstacle or the incident source is near to the sea surface or the sea floor [27-28]. Let us emphasize that the present method has just taken into account such waveguiding and multiple- scattering effects. Therefore, in practice, it is interesting in considering the ability of the proposed method to handle such multiple-scattering effects.

Both the far-field data and the scattering obstacles used in this study are outlined below: (1) the type I data and an ellipsoid B; (2) the type III data and an ellipsoid C; (3) the type V data and an ellipsoid E. For each obstacle, its reconstruction is carried out for the cases where the obstacle's centre is located at $(0, 0, h/4)$,$(0, 0, h/2)$ and $(0, 0, 3h/4)$ respectively. The reconstructions for these cases are shown in Fig. 3.3. The results show that the reconstruction based the present method is comparatively sensitive to the multiple-scattering effects generated by the waveguide boundaries. Furthermore, the results also show that such multiple-scattering effects seem to have some negative influence on the reconstruction.

Our next example shows the effects of the exterior wavenumber k, the interior wavenumber k_i and the density ratio ρ on the reconstruction. To this end, three different cases are considered: (1) for a fixed interior wavenumber k_i and a fixed density ratio ρ, varying the values of the exterior wavenumber k; (2) for a fixed exterior wavenumber k and a fixed density ratio ρ, varying the values of the interior wavenumber k_i; (3) for a fixed exterior wavenumber k and a fixed interior wavenumber k_i, varying the values of the density ratio ρ. For these results, as shown in Fig. 3.4, where the ellipsoid D centered at $(0, 0, 1/h)$ has been taken as examples, and the three types of incident and received data are considered, which are type II data, type IV data and type VI data respectively. The results show that the method works well for various values of these parameters over a reasonably wide range.

In the final set of numerical experiments, we wish to test the ability of the present method to deal with noise data. To this end, the distributed random numbers in $[-\delta, \delta]$ are added to the real and imaginary parts of the synthetic far-field data $u^\infty(\hat{x}, z; d, z_0)$ for each incident source point $(d, z_0) \in \Lambda$. We carried out the numerical experiments for the ellipsoid A centered at $(0, 0, h/2)$ and the three types of incident and received data which are type II data, type IV data and type VI data respectively. The results are presented in Fig. 3.5, where the noise level for the reconstructions is 2%. The results show that the reconstruction is sensitive to the noise in the propagation far-field data, but the proposed method has the ability of handling the

moderate amounts of noise.

4. Conclusions

To date, the numerical solution of the inverse domain problem in a shallow water waveguide has been demonstrated only in the case that the scattering object is impenetrable. The present paper has proposed an indicator sampling method for fast imaging a penetrable object in a shallow water waveguide. Moreover, it has been demonstrated that the proposed method is feasible to obtain an acceptable visualization of the penetrable object in a shallow water waveguide.

The indicator sampling method has the following interesting features in practice:

1. The imaging speed is fast since the reconstruction for a 3D object from the given propagation far-field data can be achieved in a few minutes. Moreover, the method can be very conveniently parallelized and its imaging effectiveness can be considerably increased.

2. The implementation is computationally simple since it only requires the determination of an indicator function from a linear system where the indicator function has been shown to have much larger values for points inside the scatterer than for those lying outside the obstacle.

3. No a priori information on the penetrable obstacle is required since it is not necessary to a priori know any geometrical and material properties of the penetrable obstacle.

4. The illumination and observation apertures for the unknown obstacle may be quite limited since the proposed method can succeed in producing a reasonably visualization of the unknown object even when the incidence and observation apertures are as small as the quarter of the unit cylinder surface with the half of the ocean depth.

5. The moderate amounts of noise can be handled in the reconstructions based on the proposed method. Note that it is important for many practical applications.

However, the present method has also some disadvantages. The main one is that it only provides a reconstruction of the support of the unknown obstacle and it is not possible to infer information about the fine structure of the boundary for an unknown obstacle. Nevertheless, for many practical applications, it is sufficient to acquire the support of the unknown object duo to the fact that such a support has included the abundant geometrical knowledge about the unknown object such as the number of components of the unknown object and their rough sizes, orientations and locations.

We here emphasis that our imaginary resolution performance of imaging the support of the unknown penetrable object depends on the choice of regularity parameter as if linear sampling or indicator function method did [4,5,21,26]. Although there has simple method for solving regularity parameter, it is very difficulty to implement it [29]. It can be seen that our method doesn't make it function better in ocean waveguide than in free space. On the other hand, the imaging stability doesn't depend on the measurement noise. That is we can obtain its better imaging whether the noise is added under the correct choice of regularity parameter. In [13], authors extend the optimization approach to image geometric details of an electromagnetic target that are finer than the equivalent ellipse. The cost functional measures the discrepancy between the computed and measured high-order frequency dependent polarization tensors

rather than between the generalized polarization tensors. It is shown that in the case of a high signal-to-noise ration, reconstructing fine shape information is possible. We suggest readers to refer to the paper. Moreover, it is our further work regarding this issue.

Acknowledgments. The work of the corresponding author was supported by The National Natural Science Foundation of China under grant 51073125.

References

[1] D. Colton and R. Kress, Inverse Acoustic and Electromagnetic Scattering Theory, Springer, Berlin, 1998.

[2] R. Kress, Integral equation methods in inverse acoustic and electromagnetic scattering, In Boundary Integral Formulations for Inverse Analysis, Ingham D B and Wrobel L C ed., Computational Mechanics Publications, Southampton, 1997, 67-92.

[3] D. Colton, J. Coyle, P. Monk, Recent developments in inverse acoustic scattering theory, *SIAM Rev*, **42**:3 (2000), 369-414.

[4] D. Colton, H. Haddar and M. Piana, The linear sampling method in inverse electromagnetic scattering theory, *Inverse Problems*, **19**:6 (2003),105-137.

[5] Y.X. You and G.P. Miao, An indicator sampling method for solving the inverse acoustic scattering problem from penetrable obstacles, *Inverse Problems*, **18**:3 (2002), 859-880.

[6] Y.X. You, G.P. Miao and Y.Z. Liu, A fast algorithm for visualizing multiple three dimensional objects using near-field acoustic measurements, *Acta Physica Sinca*, **50**:6 (2002), 1103-1109.

[7] Y.X. You and G.P. Miao, Acoustic far-field inversion of three-dimensional penetrable objects by an indicator sampling method, *Acta Physica Sinca*, **51**:9 (2002), 2038-2050.

[8] H. Ammari, E. Iakovleva, and H. Kang, Reconstruction of a small inclusion in a two-dimensional open waveguide, *SIAM J. Appl. Math.*, **65**:6 (2005), 2107-2127.

[9] H. Ammari, E. Iakovleva, and D. Lesselier, A MUSIC algorithm for locating small inclusions buried in a half-space from the scattering amplitude at a fixed frequency, *Multiscale Model. Simul.*, **3**:3 (2005), 597-628

[10] H. Ammari, J. Garnier, H. Kang, W.K. Park, and K. Solna, Imaging schemes for perfectly conducting cracks. *SIAM J. Appl. Math.*, **71**:1 (2001), 68-91.

[11] H. Ammari, J. Garnier, V. Jugnon, and H. Kang, Stability and resolution analysis for a topological derivative based imaging functional, *SIAM J. Control Optim.*, **50**:1 (2012), 48-76.

[12] H. Ammari, J. Garnier, H. Kang, M. Lim, and K. Solna, Multistatic imaging of extended targets, *SIAM J. Imaging Sci.*, **5**:2 (2012), 564-600.

[13] H. Ammari, H. Kang, E. Kim, and J.Y. Lee, The generalized polarization tensors for resolved imaging Part II: Shape and electromagnetic parameters reconstruction of an electromagnetic inclusion from multistatic measurements, *Math. Comp.*, **81**:278 (2012), 839-860,

[14] R.P. Gilbert and Y. Xu, The seamount problem, Nonlinear problems in applied mathematics, T. S. Angell and P. Cook et al ed., SIAM, Philadelphia, 1996, 140-149.

[15] R.P. Gilbert, Z. Lin and J.L. Buchanan, Direct and inverse problems in ocean acoustics, *Nonlinear Analysis Theor. Methods Appl.*, **30**:3 (1997), 1535-1546.

[16] C. Rozier, D. Lesselier, Z. Angell and R.F.Kleinman, Shape retrieval of an obstacle immersed in shallow water from single-frequency farfields using a complete family method, *Inverse Problems*, **13**:2 (1997), 487-508.

[17] R.P. Gilbert, T. Scotti, A. Wirgin and Y. Xu, Unidentified object problem in a shallow ocean, *J. Acoust. Soc. Am.*, **103**:3 (1998), 1320-1327.

[18] J.L. Buchanan, R.P. Gilbert, A. Wirgin and Y. Xu, Identification, by the intersecting canonical domain method of the size, shape and the depth of a soft body of revolution located within an acoustic waveguide, *Inverse Problems*, **16**:6 (2000), 1709-1726.

[19] P. Cristini and A. Wirgin, Identification of the size, proportions and locations of a soft body of revolution in a shallow-water waveguide, *Inverse Problems*, **16**:6 (2000), 1727-1739.

[20] Y. Xu, C. Mawata and W. Lin, Generalized dual space indicator method for underwater imaging, *Inverse Problems*, **16**:6 (2000), 1761-1776.

[21] Y. Xu and R.P. Gilbert, Computational results for seamount imaging in a water waveguide, *Applicable Analysis*, **82**:6 (2003), 619-628.

[22] J.L. Buchanan, R.P. Gilbert, A. Wirgin, Y. Xu, Marine Acoustics Direct and Inverse Problems, SIAM, Philadelphia, 2004.

[23] W.F. Pan, Y.X. You, G.P. Miao, Some properties on far-field pattern of scattering by penetrable obstacle in ocean waveguide, *Applied Mathematics and Mechanics*, **29**:2 (2008), 239-250.

[24] D. Colton and R. Kress, Integral Equation Methods in Scattering Theory, New York: John Wiley, 1983.

[25] T.S. Angell, X.M. Jiang and R.E. Kleinman, A distributed source method for inverse acoustic scattering, *Inverse Problems*, **13**:1 (1997), 531-545.

[26] F. Cakoni, D. Colton and H. Haddar, The linear sampling method for anisotropic media, *J. Comput. Appl. Math.*, **146**:2 (2002), 285-299.

[27] R.H. Hackman and G.S. Sammelmann, Multiple-scattering analysis for a target in an ocean waveguide, *J. Acoust. Soc. Am.*, **84**:5 (1988), 1813-1825.

[28] A. Sarkassian, Multiple-scattering effects when scattering from a target in a bounded medium, *J. Acoust. Soc. Am.*, **96**:5 (1996), 3137-3144.

[29] D. Colton, M. Piana, and R. Potthast, A simple method using Morozov's discrepancy principle for solving inverse scattering problems, *Inverse Problems*, **13**:6 (1997), 1477-1493.